

Parametric Analysis of DCE-MRI of Orthotopic Lung Cancer

Y. Rosen¹, H. Degani¹, R. Margalit¹, D. Grobgeld¹, E. Furman-Haran¹

¹Biological Regulation, Weizmann Institute of Science, Rehovot, Israel

Introduction

Lung cancer is the leading cause of cancer death worldwide, and 80% of the cases are non-small cell lung carcinoma (NSCLC) (1). The poor survival rates are related to late detection, usually at a stage when the tumor is already unresectable. Thus far, animal models of orthotopic lung cancer were rarely investigated by MRI, mainly because of the necessity to compensate for motion produced by respiration at high rates. In this study we describe dynamic contrast enhanced (DCE) MRI experiments performed on animal models of orthotopic human lung cancer, and present various approaches of image analysis that provide assessment of the vascular characteristics of this type of cancer.

Methods

NCI-H460 human NSCLC cells were implanted in the lungs of female nude rats by intrabronchial injection, as previously described (2). All animal procedures were approved by IACUC.

MR images were recorded with a 4.7T Biospec spectrometer (Bruker, Germany). The DCE-MRI experiments were performed by a 3D-GE T1-weighted imaging sequence, with TE/TR=2.1/25msec, $\alpha=60^\circ$, $0.234 \times 0.469 \times 2.5 \text{ mm}^3$ voxels (coronal), and 1 minute temporal resolution. Images were acquired before and consecutively for 20 minutes after a bolus injection of 0.1 mmol/kg Gd-DTPA into the tail vein.

The arterial input function of Gd-DTPA in the plasma of nude rats was calculated by fitting the signal enhancement curves of regions of interest (ROI's) at the heart ventricle or in one of the great vessels, taking into account the hematocrit value, to the bi-exponential decay: $C_p = D * (a_1 * \exp(m_1 t) + a_2 * \exp(m_2 t))$ (3). Final values for a_1 , m_1 , a_2 , and m_2 were averaged from 3 rats.

Two different analysis approaches were investigated in order to compensate for motion between images in the dynamic series of the tumors,

1. Analysis of global slice enhancement patterns: A tumor's ROI was defined for each tumor slice, and a global signal intensity at each time-point was averaged from pixels in this ROI that were enhanced by more than 30% at the first post-contrast measurement (0.5min), producing a global enhancement curve for each tumor slice.

2. Image registration followed by pixel-by-pixel analysis of the enhancement curves: All post-contrast images were registered to the pre-contrast image. Image registration was applied by using the FMRIB's Linear Image Registration Tool (FLIRT) of the FMRIB Software Library (FSL) version 3.1 (4). The 3D registration was performed with 9 degrees of freedom, using the correlation ratio cost function. The cost function was weighted so that the region of the tumor had 10-fold higher weight than the remainder of the image.

All enhancement curves were analyzed by applying a nonlinear curve-fitting algorithm to yield separate parametric maps for the influx transcapillary transfer constant, k_{in} , the efflux transcapillary transfer rate constant, k_{ep} , and the ratio k_{in}/k_{ep} related to the extra-cellular volume fraction accessible to the contrast agent, v_e , using the physiological model of Tofts (5).

Results

Tumors were followed for up to 25 days, reaching a volume ranging from 0.19 to 2.18 cm^3 .

The pharmacokinetic parameters found for Gd-DTPA in the nude rats were: $a_1 = 9.44 \pm 2.7 \text{ kg/l}$, $m_1 = 0.756 \pm 0.21 \text{ min}^{-1}$, $a_2 = 3.99 \pm 1.63 \text{ kg/l}$, $m_2 = 0.033 \pm 0.01 \text{ min}^{-1}$ (n=5).

Global enhancement curves of the tumors' slices were determined from average signal intensities of tumor pixels that followed the aforementioned criterion of exceeding 30% enhancement at the first post-contrast time-point. An average of $76.9\% \pm 9.8\%$ of the tumor pixels entered the calculations. These pixels were spread throughout the tumor without any typical distribution pattern. Curve fitting of the average signal enhancement resulted in: $k_{in} = 0.39 \pm 0.22 \text{ min}^{-1}$, $k_{ep} = 1.52 \pm 0.83 \text{ min}^{-1}$, $v_e = 0.27 \pm 0.07$, with R^2 values of 0.77 ± 0.08 (n = 6 tumors with 14 slices).

Fitting the pixel enhancement curves to Tofts' model produced parametric maps of k_{in} , k_{ep} and v_e for each tumor slice (fig. 1). The registered set of dynamic images showed a better fitting demonstrated by higher R^2 values than those obtained for the same set of un-registered images ($P < 0.05$), hence more pixels entered the statistical analysis. This analysis included about 40% of tumor pixels (with $R^2 > 0.5$), distributed throughout the whole tumor volume, without a typical rim or any other enhancement pattern. Median values of the perfusion parameters were: $k_{in} = 0.49 \pm 0.33 \text{ min}^{-1}$, $k_{ep} = 1.42 \pm 0.82 \text{ min}^{-1}$, and $v_e = 0.34 \pm 0.09$ (n = 6 tumors with 14 slices).

Statistical analysis of the transcapillary transfer constants showed that median pixel k_{in} and k_{ep} values were not significantly different from global slice values ($P > 0.05$) (2-tailed, paired t-test). Good correlation was found between the parameter values measured by the two analysis techniques: 0.82 and 0.81 for k_{in} and k_{ep} respectively (Pearson correlation test, fig. 2).

The transcapillary transfer constants in the orthotopic lung tumors were found to be an order of magnitude higher than those measured in the same type of tumors implanted subcutaneously (data not shown) or in other human subcutaneous tumor xenografts (6).

Conclusions

In this study we showed that orthotopic human lung cancer animal models can serve for investigating tumor vascular characteristics by DCE-MRI. Although motion is a serious drawback, analysis of global enhancement and image registration can provide physiologically relevant results. The orthotopic lung tumors do not show a typical rim enhancement, and they are characterized by an order of magnitude higher values of transcapillary transfer constants than subcutaneously implanted human tumors. These findings may be explained by richer vascularization and better drainage in the lung as well as increased pathological angiogenic activity in the microenvironment of lung cancer.

References: 1) Billello KS *et al. Clin Chest Med* 2002, 23(1):1-25. 2) Howard RB *et al. Cancer Res* 1991, 51(12):3274-80. 3) Weinmann HJ *et al. Physiol Chem Phys Med NMR* 1984,16(2):167-72. 4) Jenkinson, M, Smith S. *Medical Image Analysis* 2001, 5(2):143-156. 5) Tofts, PS. *J Magn Reson Imaging* 1997, 7(1):91-101. 6) Checkley D. *et al. Magn Reson Imaging*. 2003, 21(5):475-82.

Supported by: Ms. Edith Degani and Mochon Family; ISF grant 801/04; Estate of Julie Osler, USA.

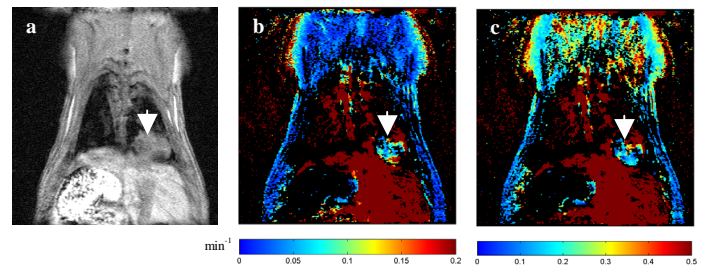


Fig. 1 a) MR image acquired 7 minutes post contrast administration, showing a tumor in the right lower lobe. b,c) Parametric maps of k_{in} and k_{ep} respectively. The tumor is marked by an arrow.

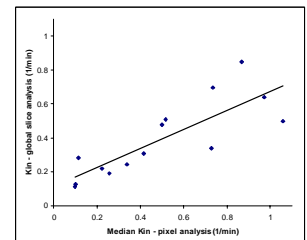


Fig. 2 Correlation between k_{in} from global analysis and median pixel k_{in} of the same slice. Correlation ratio : 0.82 (14 slices of 6 tumors).